

## Dual-scale approach for detection of tsunami-affected areas using optical satellite images

T. T. VU\*†, M. MATSUOKA‡ and F. YAMAZAKI†

†Department of Urban Environment Systems, Faculty of Engineering, Chiba University, Japan

‡Earthquake Disaster Mitigation Research Center (EDM), National Research Institute for Earth Science and Disaster Prevention, Japan

As various sensors with different spatial resolutions, spectral resolutions, etc., have been in operation, an extremely large image database is ready. How to retrieve the relevant information is a critical problem in the context of quick damage assessment. This study develops a framework to integrate medium resolution (Landsat or ASTER) and high-resolution (QuickBird or IKONOS) satellite images and digital elevation data in mapping tsunami-affected areas. The processing flows upwards from macro-scale (medium spatial resolution data) to micro-scale (high spatial resolution data). Across this pyramidal searching, only necessary data is acquired, processed and the focused geographical extent is narrowed. Suitable pixel-based and object-based processing methods are also developed. Using the developed processing flow drastically reduces acquisition cost and processing time. The selected test sites in Phangnga and Phuket Provinces, Thailand, which were severely affected by the 2004 Indian Ocean tsunami, are used to demonstrate the performance of the framework. Further studies include the implementation of the processing system and the extension of the idea to other natural hazards.

### 1. Introduction

For decades, remote sensing techniques have been extensively exploited in hazard mapping and disaster mitigation. To quickly map a large affected area to be used for damage assessment and coordination of relief efforts, remote sensing is the only capable technique. There have been plenty of published works and real implementations of remote sensing in hazard mapping. A few examples are flood mapping (Barber *et al.* 1996), displacement mapping due to earthquakes (Massonnet *et al.* 1993), earthquake damage detection (Matsuoka and Yamazaki 1999), landslide mapping (Singhroy and Mattar 2000, Vohora and Donoghue 2004) and volcano observation (Mouginis-Mark *et al.* 1991, Andres and Rose 1995). The development of advanced remote sensing technologies have improved the mapping capabilities and expanded the areas of application. The most significant improvement was the commercialization of high spatial resolution satellite images such as IKONOS and QuickBird. They have been employed in earthquake damage detection (Vu *et al.* 2005, Yamazaki *et al.* 2005) or landslide mapping (Vohora and Donoghue 2004), etc. Depending on the nature of the catastrophe and the

---

\*Corresponding author. Email: thuyvu@as.tu.chiba-u.ac.jp

availability of satellite data, one or some kinds of satellite images are acquired and analysed. In addition, the selection of the relevant satellite image also depends on the analyst's expertise; 'which satellite data must be used?' and 'which methodology is suitable?' are very crucial.

Advancements in remote sensing technologies have resulted in an increase in the size and complexity of image databases. Therefore, choosing the relevant image data is not a simple task. In the context of damage mapping, two image datasets must be retrieved. They are the pre-event dataset and the post-event dataset. It is noted here, that there is also a damage mapping approach concerning only post-event datasets (Mitomi *et al.* 2001). Although research on retrieval of images from large databases has been a focus for the computer vision community for some time it has recently become a focus for the remote sensing community (Castelli *et al.* 1998, Agouris *et al.* 1999). The content-based approach is found to be more suitable for dealing with geographical information contained in the images. These approaches can be employed to retrieve the inventory image data. However, the present study focuses on retrieval of image data after a catastrophe occurs when the content has been changed. The only available clue is the geographical information, i.e. location and some extents. In addition, computational time is essential for quick damage assessment. A simple but efficient approach to retrieve less redundant information is required and the appropriate solution depends on the type of disaster, in our case the paper focuses on the Indian Ocean tsunami which was caused by an earthquake.

A magnitude  $M_w=9.0$  earthquake (US Geological Survey) occurred off the coast of Sumatra, Indonesia on 26 December 2004 and the triggered tsunami caused massive devastation in vast areas along the coastlines of the Indian Ocean. For this awful catastrophe, all the existing satellites – coarse resolution like MODIS, medium resolution like ASTER, and high resolution like QuickBird – tried to capture images of the affected areas. Consequently, the question about the availability of one kind of satellite image did not need to be concerned. The problem was turned into finding an efficient solution to quickly grasp the necessary information, i.e. the maps of the affected areas. Obviously, there is a trade-off between the total cost including data acquisition and computational time and the level of detail. Based on the facts of this massive tsunami and the experiences from previous catastrophes such as the 1995 Kobe, Japan earthquake (Matsuoka and Yamazaki 1999), the 1999 Kocaeli, Turkey earthquake (Eguchi *et al.* 2000, Estrada *et al.* 2000), the 2001 Gujarat, India earthquake (Mitomi *et al.* 2001, Saito *et al.* 2004), the 2003 Bam, Iran earthquake (Vu *et al.* 2005, Yamazaki *et al.* 2005), it was realized that scale was a crucial factor. It is also after considering other studies on retrieval of images from large database (Castelli *et al.* 1998). Exploiting the scale properties in developing an integrated framework can be a cost-effective solution to using remotely sensed data in quick hazard mapping and damage assessment.

An integrated processing framework for medium spatial resolution optical satellite images (Landsat or ASTER), high spatial resolution optical satellite images (QuickBird or IKONOS) and digital elevation data in detection of tsunami-affected areas is developed. The processing flow moves upwards from macro-scale (medium resolution data) to micro-scale (high resolution data). The key point of this framework lies in processing only necessary data to provide just enough information. High-resolution data is required only when analysed results on macro-scale could not provide enough information or the site is of a specific

concern. The following section describes the idea of dual-scale mapping applied in mapping tsunami-affected areas. It is followed by descriptions of detailed processing on macro- and micro-scales using satellite images acquired over the tsunami-affected areas in the south of Thailand. It should be noted that the developed framework in this study is limited to optical satellite images. Radar images might be included in future developments of the framework.

## 2. Dual-scale mapping of tsunami-affected areas

Objects in the world appear in ways that depend on the scale of observation (Lindeberg 1993). Satellite images present the overlaying objects on the Earth's surface depending on the design of satellite sensors. Therefore, satellite images acquired by different sensors present an object in different ways. As a result, the level of detail and the extent of a scene differ. For instance, a Landsat multi-spectral scene covers an area of  $185 \times 172 \text{ km}^2$  with 30 m spatial resolution and a QuickBird scene covers an area of  $16.5 \times 16.5 \text{ km}^2$  with 2.4 m spatial resolution. It is fast and easy to figure out the extent of a catastrophe by using coarser images but not in detail. On the contrary, it is very costly and time consuming to cover the entire affected areas only by high spatial resolution images. For quick mapping, the trade-off between these factors should be considered. A framework to integrate data on two different scales is proposed as described below. Because the study focuses on processing satellite images, data also means image in this paper.

Figure 1 demonstrates the simple idea of dual-scale mapping. Starting from a macro-scale, a set of algorithms to search data and to detect affected areas is applied. Let  $S$  be a detected set on a macro-scale and  $B$  be a subset of  $S$ , i.e.  $B \subseteq S$ . Because  $B$  is with specific concern for more detailed mapping, its geographic extent is mapped in micro-scale in order to search for the corresponding data on this scale. Subsequently, micro-scale detection algorithms are applied. It is obvious to estimate how much the acquisition cost can be reduced by using this dual-scale link. Moreover, the micro-scale algorithms are generally much more complicated than the macro-scale ones. The dual-scale mapping carries out such complicated micro-scale algorithms to a smaller extent.

Theoretically, a tsunami is triggered by a big earthquake of magnitude higher than  $M_w=6.5$  which generates displacement of seabed. It attacks the coastal zone

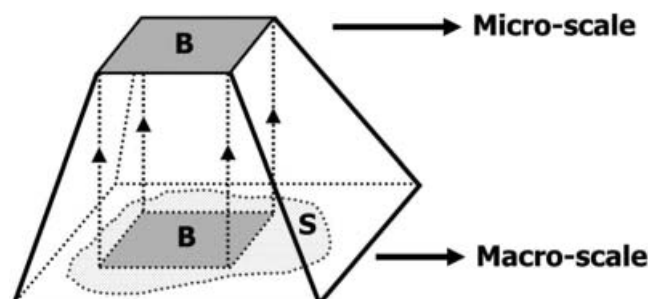


Figure 1. Schematic plot of the dual-scale mapping idea.  $B$  is the selected area for micro-scale analysis out of the area  $S$  for macro-scale analysis.

and washes away buildings, trees, etc. along the coastline. The extent of affected areas depends on the topography of the coastal zone as well as the three-dimensional (3D) configuration of seabed. From these observations, the dual-scale mapping of tsunami-affected areas was designed as shown in figure 2. Firstly, medium resolution satellite images of the affected coverage are acquired. The pre-event scene is used to detect the coastline. It can be easily done solely by thresholding the near-infrared (NIR) band or applying the K-mean unsupervised classification followed by the extraction of water class. Using the detected coastline, a proximity analysis with 8-connectivity is carried out to generate a 'less than 1.5 km distance' map. This is due to past experiences, i.e. a tsunami does not go up farther than this distance once it reaches land. But we must be careful to remember that tsunami may go up much farther along rivers. A 90 m digital elevation model (DEM) grid derived from Shuttle Radar Topography Mission (SRTM) is also employed. The areas lower than 20 m are selected as potentially affected areas. These two selected classes form the first draft geographic extent.

The macro-scale analysis is designed to use all remotely sensed data between 10 m and 30 m spatial resolution like ASTER, Landsat and SPOT. As mentioned above, tsunami is usually restricted in a thin belt along the coastline; coarser spatial resolution satellite imagery like MODIS will not clearly present the affected areas. The geographic extent formed by the distance map and elevation threshold narrows the processing space of the medium resolution satellite images. Comparison of Normalized Difference Vegetation Index (NDVI) is the main processing on this scale and the details are presented in §4.

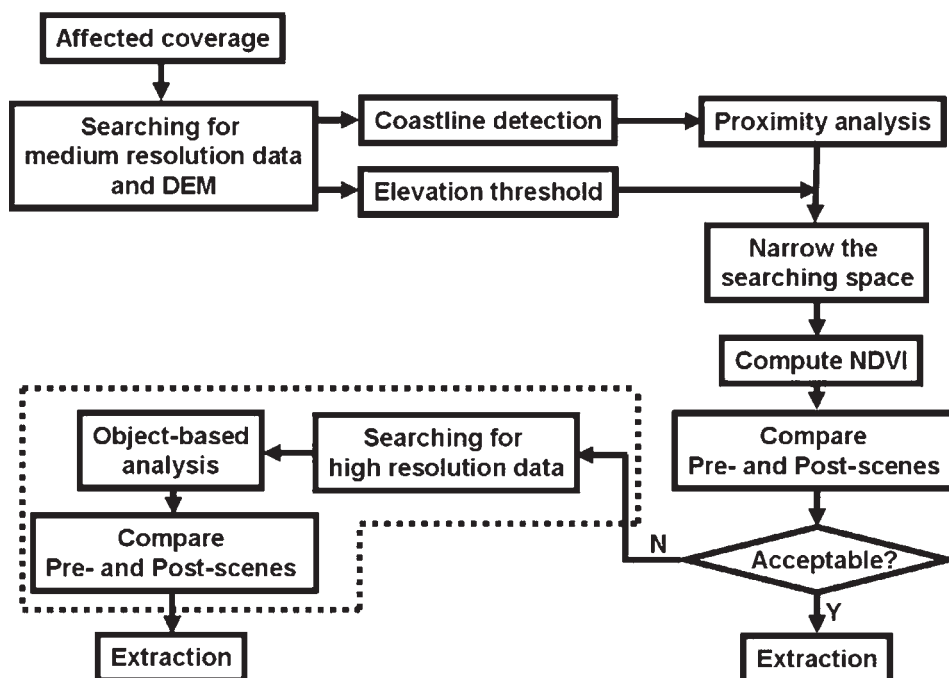


Figure 2. Flow-chart of proposed dual-scale image processing.

On micro-scale, high spatial resolution satellite images such as QuickBird and IKONOS are employed. For a <1m resolution image of a small focused extent, visual interpretation is applicable. However, an automatic object-based approach was also developed for this detailed mapping. Detailed micro-scale processing is described in §5. In both, macro- and micro-scale processing, several algorithms were developed based on area morphology. Its theory and employment in our image processing are presented in §3.

### 3. Area morphology in image processing

Serra (1982) first introduced mathematical morphology. Conventional morphological operations include dilation, erosion, opening, closing, etc. applying a structure element with a specific shape and size to an image in order to filter out the unwanted or obtain the wanted information. Such morphological operations and their combination can accomplish many tasks of image processing. However, as the object shapes are often unknown and diverse in an analysed image, especially in remotely sensed images, this operation is hardly applied in every case. One solution is applying a series of operations but it is computationally intensive. Also 'greyscale reconstruction' or 'geodesic method' is a possible solution to overcome the problem (Lantuejoul and Maisonneuve 1984, Vincent 1992). Initiated from this, Vincent (1992) introduced the idea of area openings and closings.

#### 3.1 Area morphological filtering

Area opening filtering removes the components with an area smaller than a parameter  $s$  from a binary image. Similarly, area closing filtering fills the holes with an area smaller than a parameter  $s$ . The binary area opening is defined as follows. Let  $X$  be a subset of set  $M \subseteq R^2$  and  $\{X_i\}$  is all the connected components of  $X$ . The area opening of parameter  $s$  ( $s \geq 0$ ) of  $X$  is the union of the connected components of  $X$  with area greater than  $s$ :

$$\gamma_s^a(X) = \cup \{X_i | i \in I, \text{area}(X_i) \geq s\} \quad (1)$$

The area closing of parameter  $s$  ( $s \geq 0$ ) of  $X$  is then defined as:

$$\phi_s^a(X) = [\gamma_s^a(X^C)]^C \quad (2)$$

where  $X^C$  denotes the complement of  $X$  in  $M$

Vincent (1992) then extended the definition of binary area opening or closing to greyscale area opening or closing. A greyscale image can be defined as a mapping  $f: M \rightarrow R$ . The greyscale opening of  $f$  is given by:

$$(\gamma_s^a(f))(x) = \vee \{h \leq f(x) | x \in \gamma_s^a(T_h(f))\} \quad (3)$$

where  $\vee$  stands for supremum, i.e. a lowest upper bound, and  $T_h$  is the threshold of  $f$  at value  $h$ .

$$T_h(f) = \{x \in M | f(x) \geq h\} \quad (4)$$

In other words, the image  $M$  is firstly threshold with all the possible  $h$  and the binary opening  $\gamma_s^a(T_h(f))$  is found. Subsequently,  $\vee$  is applied to all the recently found  $\gamma_s^a(T_h(f))$ . It is similarly extended to greyscale closing by duality. Area morphological filtering does not depend on the shape of structural elements as

the conventional ones. Therefore, it can effectively remove noise and simultaneously retain thin or elongated objects.

### 3.2 Area morphological classification and feature extraction

The area opening and closing for greyscale images are flat increasing mapping which can be used for image simplification (Soille and Pesaresi 2002). An example of image simplification is shown in figure 3, where a greyscale area opening followed by a greyscale area closing opening was applied to a QuickBird image with parameter of 1000 pixels. This filtered image can assist visual interpretation or can be extended to classification or feature extraction.

The conventional classification methods, either supervised or unsupervised, categorize the spectral signatures into different groups. Only statistical information of spectral signatures is included. The form and structure of objects are not considered. As a result, the classified images represent a number of sets of pixels assigned to different classes. For further usage of the result, e.g. input to GIS database, post-processing is required. These conventional methods can generate a reasonably classified result for coarse to medium spatial resolution images because these images do not possess enough structural information either. However, high spatial resolution satellite images possess very detailed information. More signatures should be included in their classification.

Area morphology is exploited to classify high spatial resolution satellite images across the scale space. Morphological information of an object depends on scale property. Classification across the scale space is the solution to integrate morphological information with spectral information. K-mean clustering algorithm (Tou and Gonzalez 1974) is employed to group the pixels across the scale space and the spectral space. Step-by-step scale space clustering classification is described next.

Theoretically, the scale space is generated by an infinite number of scales. For the discrete dimension of an image, the number of scales increases one each as a window (area) size increases from one pixel to an image size. However, it is

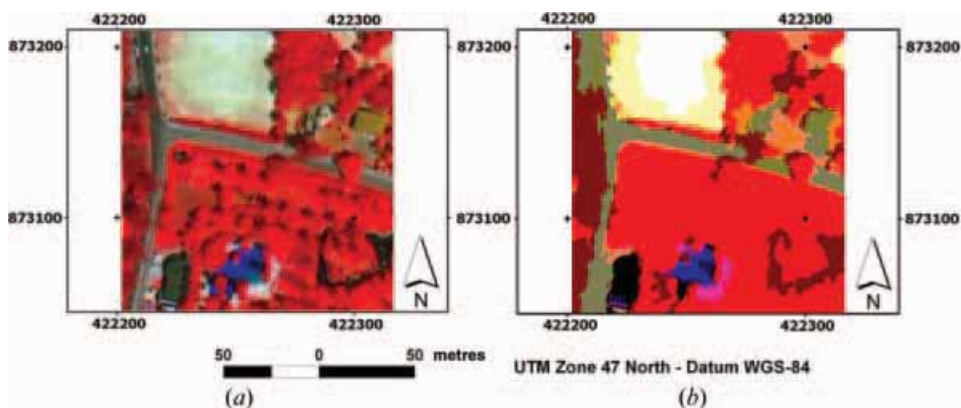


Figure 3. An example of image simplification by greyscale area opening and closing; original false colour composite image (a) and filtered false colour composite image with scale parameter  $s=1\ 000$  (b).

time-consuming to concern all the area values. Practically, a scene contains a limited number of sizes. Therefore, in the first step, horizontal and vertical granulometry analyses (Vincent 1994) are carried out to find the potential patterns contained in an image as illustrated in figure 4. The local maximum found in horizontal and vertical dimensions can be used to compute the possible areas of objects in the image. Computed areas are parameters for scale space generation. If a single-band image is analysed, granulometry analysis runs on this image. Alternatively, when a multi-spectral image is analysed, to be simplified, granulometry analysis runs on the first component image derived from Principle Component Analysis (PCA).

Secondly, area opening followed by area closing with the above defined area parameters is carried out on each band. This step is extremely time consuming if there are many scales to be analysed and the pixel values are in a wide range. Parallel processing is a good solution since the processing can independently run for each grey value and also each band. Moreover, narrowing the range of grey value can also reduce the computational time. To maintain the distribution of grey value well, division of a band by its standard deviation is employed. The second step opens a single-band image to its scale space. The products of this step in true colour composite or false colour composite are useful in assisting visual interpretation.

The third step is to cluster the spectral signatures by K-mean algorithm (Tou and Gonzalez 1974). K-mean algorithm is an iterative process which minimizes the distance from an entity to the centre of a cluster. At every step of the iteration, the centres of the clusters are recomputed. The attributes used for this clustering are

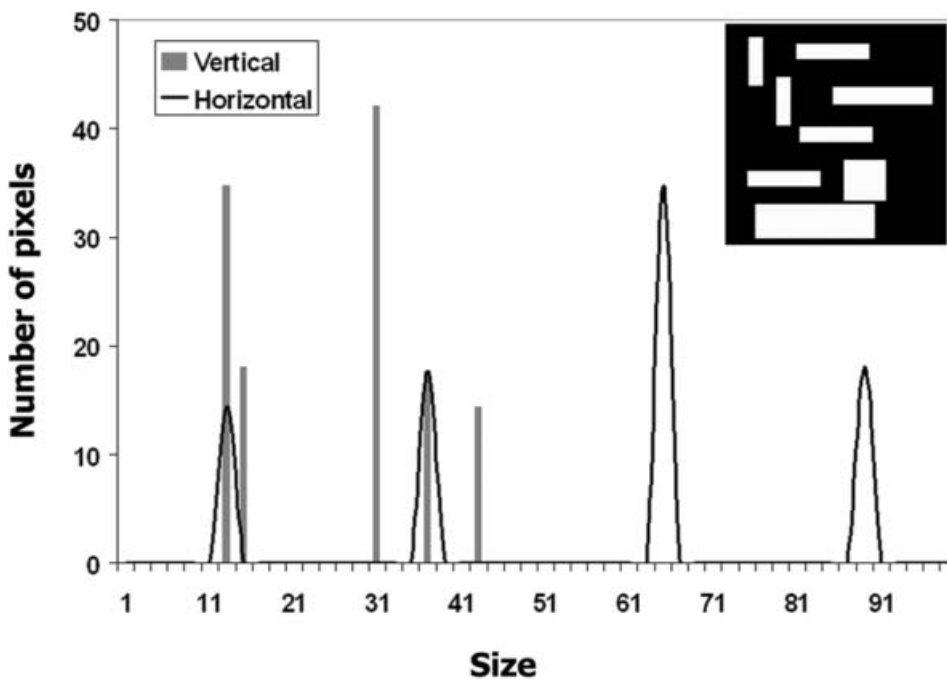


Figure 4. Illustration of the horizontal and vertical granulometry analyses.

the spectral signatures. Let  $I_{is}$  be the grey value of pixel  $i$  at channel  $s$  ( $s = 1, 2, \dots$ , the number of channels).  $I_i = \{I_{is}\}$  is called the spectral vector of pixel  $i$ . The clustering compares and assigns classes according to similarity of this spectral vector of every pixel. It should be noted that not all the scales should be clustered. Generally, very coarse scales reflect ground objects which are assumed to be background. In classification or segmentation of buildings, trees, etc., those scales might be excluded. In addition, a very fine scale might also be excluded if it stands for very small objects which can be assumed noise. This step separately generates clustered objects on each chosen scale.

Across the scale space from fine to coarse scale, an object with a certain area is absorbed into a bigger one. Starting from a very coarse scale and moving upwards to finer ones, as soon as a new object appears inside a current one, it is the cue to extract this new small object. For illustration, an example of the segmented results from an original image (figure 5(a)) in false colour composite on three consecutive scales is presented from finer to coarser scales in figure 5(b) to 5(d).

Depending on the defined scale parameters and assigned numbers of classes, the final classified image represents the objects with an assigned class rather than a set of pixels by conventional classification. The classification or segmentation based on area morphology analyses spectral signatures in a morphological frame. It maintains structural information in the neighbour while analysing spectral information. Very complex scenes in urban areas, such as complex structures including many small parts with diverse spectral signatures or a street partly hidden by trees, might not be segmented as one. Post-processing, either by visual inspection or knowledge-based from a current database, is required for such cases.

#### 4. Macro-scale processing

Two ASTER pairs of Khao Lak, Phangnga Province and Patong, Phuket Province are used to demonstrate the macro-scale processing. Their acquisition dates are shown in table 1. The pre-event and post-event Khao Lak ASTER images in false colour composite are shown in figure 6(a) and 6(b), respectively. It is easy to observe the affected areas due to massive devastation of vegetation along the coastline. The corresponding NDVI signatures were computed and they are shown in figure 6(c) and 6(d), respectively. Computation was carried out for a smaller extent defined by the window generated by elevation and distance thresholds (figure 7(a)). As vegetation was washed away by the tsunami, the NDVI values of the affected zones were reduced. Therefore, thresholding the difference between pre-NDVI and post-NDVI values shows the potentially affected zones. Let  $preNDVI$  and  $postNDVI$  are the computed NDVI values from the pre-event and post-event images, respectively. The potentially affected zones  $pZ$  are defined by:

$$pZ = \{Z_i | (Z_i \in DIFF) \text{ and } (val(Z_i) < Mean(DIFF) - Std(DIFF))\} \quad (5)$$

where  $DIFF$  is the set generated by  $postNDVI - preNDVI$ ,  $Z_i$  is a pixel,  $val(Z_i)$  is its value and  $Mean(DIFF)$  and  $Std(DIFF)$  are the average and standard deviation values of  $DIFF$ , respectively.

The affected zones that were extracted by the above statistical threshold are shown figure 7(b). Then, binary area opening and closing filtering with a parameter of 100 was applied to figure 7(b) and the affected zones were extracted as shown in figure 7(c). The detected zones, which were in raster format, were then converted to vector format for further usages.

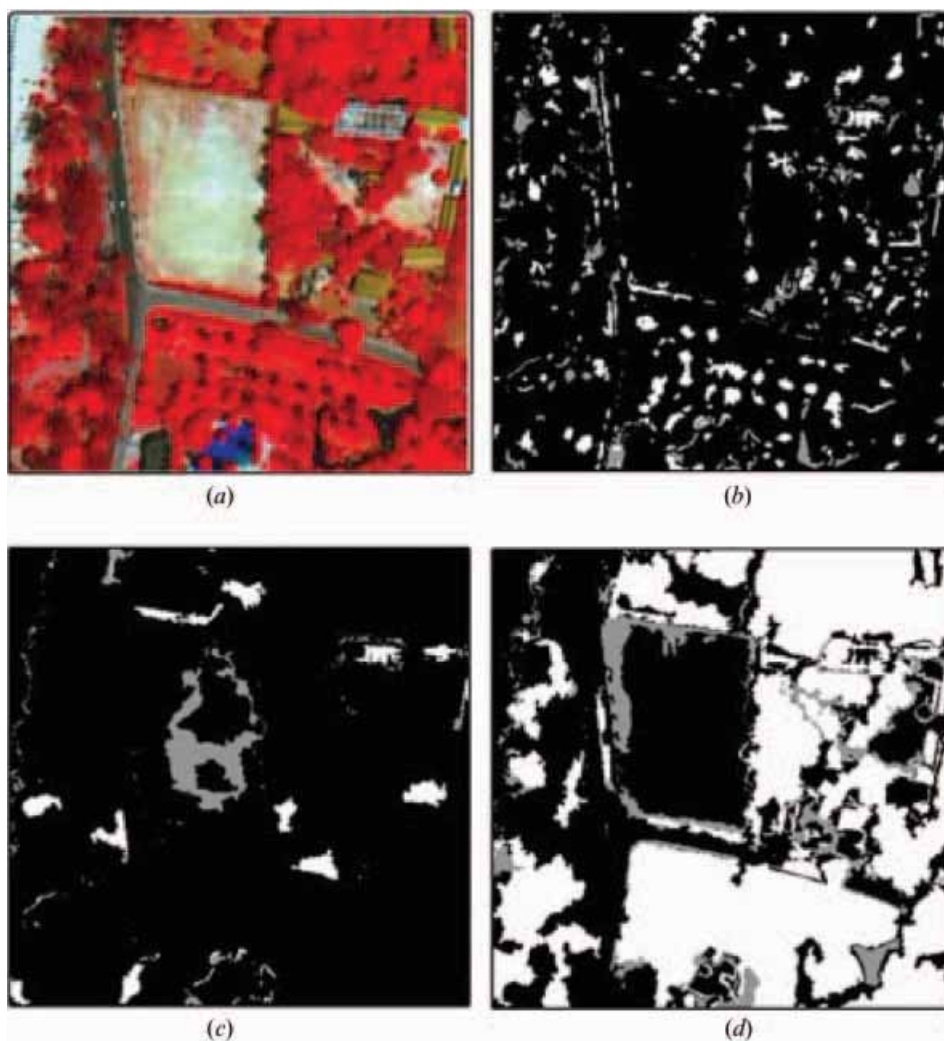


Figure 5. Illustration of segmentation; (a) is the original false colour composite and segmented results on three parameter scales from fine to coarse are shown in (b) for  $s=9$ , (c) for  $s=300$  and (d) for  $s=510$  (black is the background and greyscale code for different spectral classes).

Two scenes acquired over Khao Lak were in the same season. Therefore, simple comparison of NDVI was successful. Searching the archive data to retrieve the pre-event scene, which is in the same season as the post-event scene, is required. There

Table 1. ASTER images used during macro-scale analysis.

	Khao Lak, Phangnga	Patong, Phuket
Pre-event	15 November 2002	28 February 2003
Post-event	31 December 2004	31 December 2004

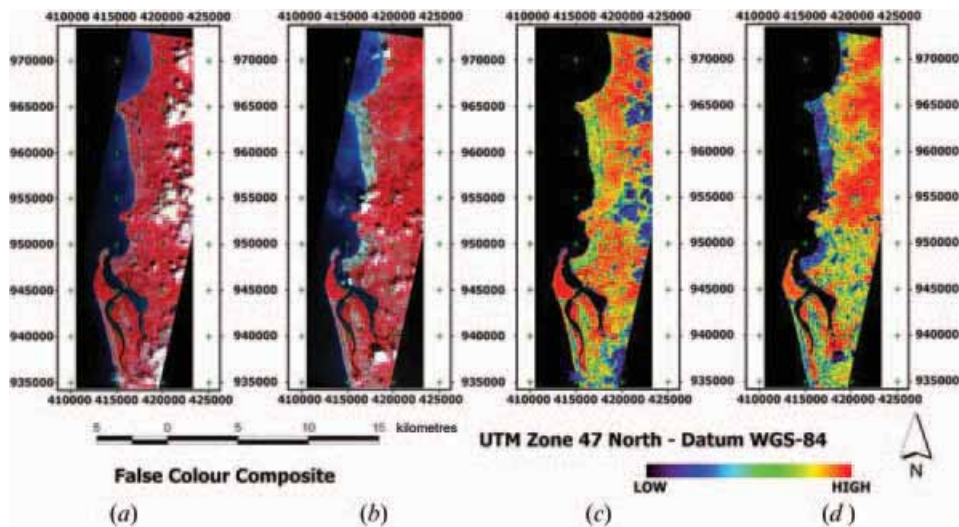


Figure 6. False colour composite for pre-event (a) and post-event (b) ASTER images for Khao Lak and corresponding NDVI signatures for pre-event (c) and post-event (d).

are some errors due to cloud cover, which can be removed easily and quickly. The biggest obstacle in detecting tsunami-affected zones, as well as the ones due to other natural hazards, is man-made changes. As observed in figures 6 and 7, there are a

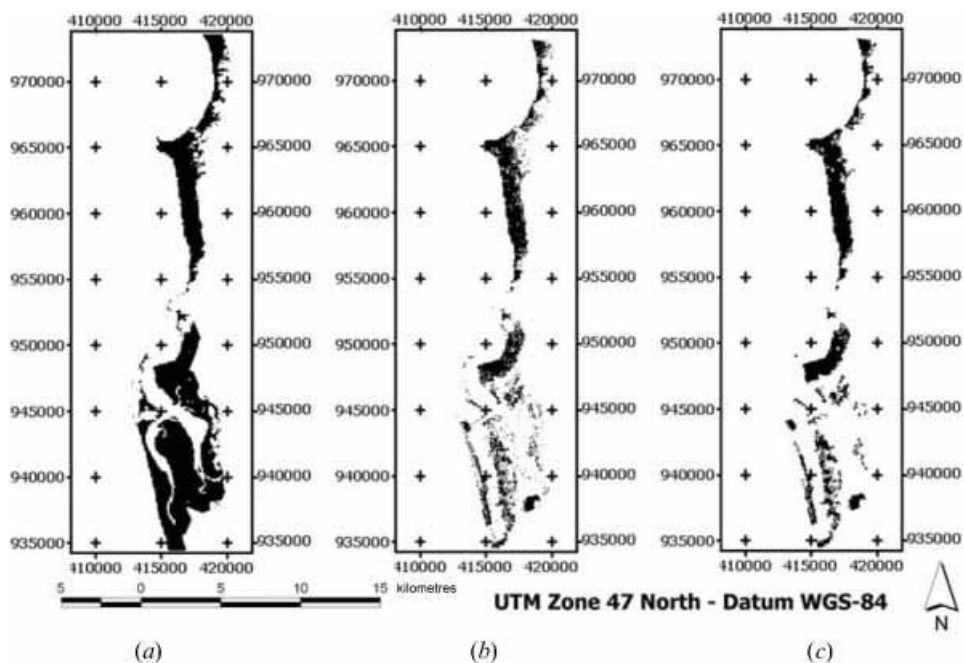


Figure 7. (a) Selected areas by elevation and distance thresholds. (b) Extracted affected zones. (c) Filtered extracted affected zones.

few detected polygons not due to tsunami. They are usually far away from the seashore. If not, these cannot be distinguished automatically; in such cases visual inspection is required. To eliminate the detected polygons due to man-made changes and far away from the seashore, proximity is checked as follows. Let  $Z$  be the set of detected polygons, i.e.  $Z = \{Z_i\}$  and  $S$  is the sea class. The newly detected set of affected zones is given by:

$$A = \{Z_i | Z_i \text{ is neighbour of } S\} \quad (6)$$

The extraction affected areas from the pre-event and post-event ASTER images of Patong, Phuket, however, showed no clear differences between the images even though Patong is one of the areas hit hardest by the tsunami. It means that ASTER is unable to detect affected areas in Patong using medium resolution satellite images or, in other words, macro-scale. There are a lot of buildings and other structures along the coastline catering for tourism. The tsunami was blocked by those structures and could not reach too far inland. Although the tsunami destroyed those structures, this was not observed in the moderate-resolution satellite images, i.e. top-view. Micro-scale mapping might provide more information. The selected extent from the ASTER image for searching high-resolution satellite images were (421 700, 874 100) at the top-left corner and (424 400, 872 300) at the bottom-right corner. The coordinates were presented in UTM projection, zone 47 North.

### 5. Micro-scale processing

Following the extracted extent above, pre-event and post-event QuickBird images of Patong were purchased as listed in table 2. These two images were acquired in the same dry season. However, there is a three-year difference in acquisition time during which some man-made changes may have taken place. Furthermore, cloud cover also limits the corresponding extent between the two images. Because of the complex and detailed information observed on micro-scale, both, visual and automated interpretation methods were introduced assisted by area morphology (see §3.2). Prior to that, pan-sharpening was carried out to exploit multi-spectral information at the better spatial resolution of 0.6 m instead of 2.4 m.

As pointed out by Zhang (2002), conventional pan-sharpening algorithms such as IHS fusion, PCA fusion, etc. were developed for the satellite images whose panchromatic channel covers only the visible regions of the electromagnetic spectrum. Thus, such algorithms do not work well for high-resolution satellite images like QuickBird and IKONOS. An improvement can be achieved by adjusting the contribution from the panchromatic band when pan-sharpening other multi-spectral band images, depending on sensor characteristics and the covered area. However, it is quite difficult to clearly analyse the contribution from the panchromatic band to each multi-spectral band due to inter-correlation among

Table 2. QuickBird images used during micro-scale analysis.

	Patong, Phuket
Pre-event	23 March 2002
Post-event	02 January 2005

them. We propose an improved pan-sharpening method based on PCA named *PCPANfit* as follows.

First, multi-spectral scenes are re-sampled using the same spatial resolution as the corresponding panchromatic scenes. They are then extracted in the same extent. Second, forward PCA transformation is applied to the multi-spectral channel images. The histogram of the panchromatic channel image is adjusted to be the same scale as that of the first component by PCA. The adjusted panchromatic channel then replaces the first component. Third, reverse PCA transformation is carried out. Subsequently, a regression analysis is applied to find out a possible relationship between each newly formed channel and each original multi-spectral channel. Last, the grey value of each channel is adjusted following the relationship to obtain the final pan-sharpened image. All the steps are developed in one module and a user is required to input only original panchromatic and multi-spectral channel images. A test of this *PCPANfit* for a 1200 pixel  $\times$  1200 pixel QuickBird scene with four multi-spectral bands on a Windows-based desktop PC with 3.06GHz CPU and 2GB RAM took only 15 second. It generated a good-look pan-sharpened image with less colour distortion. The correlation coefficients between this pan-sharpened image and the original multi-spectral images were 0.86, 0.85, 0.85 and 0.90 for blue, green, red and NIR bands, respectively.

The panchromatic scene described above was used in granulometry analysis to investigate potential pattern areas in the scene. The analysis on the pre-event panchromatic scene showed that the possible area parameters are 9, 300, 510, 1 167, 17 000 and 38 700. These six area parameters were used to generate the scale space. The post-event scene, due to the effect of the tsunami attack, was expected to contain more object classes. In addition, possible man-made changes might also introduce several different area parameters. As the scene has not completely changed, the area parameters found from the pre-event scene still represent the areas in the post-event scene. The same parameters, hence, were used for both scenes. It is also meaningful to apply a predefined set of parameters derived from archive data, i.e. pre-event data, to a newly acquired post-event scene in the context of quick damage assessment.

For illustration, figure 8 shows a selected affected area in false colour composite images on scales  $s=9$ , 510 and 17 000 compared to its original false colour composite. Human perception can easily understand and map the affected areas in the spatial resolution of 0.6 m. However, extraction is made easier with the assistance of information across the scale space. For example, trees can be extracted on scale 9 and inundated areas with mud or sand brought by tsunami can be extracted on scale 510. Based on this, affected zones can be extracted and overlaid on other layers in further assessment. In this processing framework on micro-scale, we also employed the area morphological classification as described in §3.2. It provides a higher level of automation.

The treated area morphological classification entity is the object whose properties are spectral class and the range of size rather than the pixel by conventional methods. Objects were extracted from the pre-event scene depending on their spectral and structural information. The segmented results from the pre-event image were all converted to vector format. Each segmented object became a polygon with range of sizes and spectral class as its attributes. They are readily used to update or develop a GIS database. To segment a post-event scene, new sets of parameters must be derived by granulometry analysis and the same scheme as applied to the pre-event

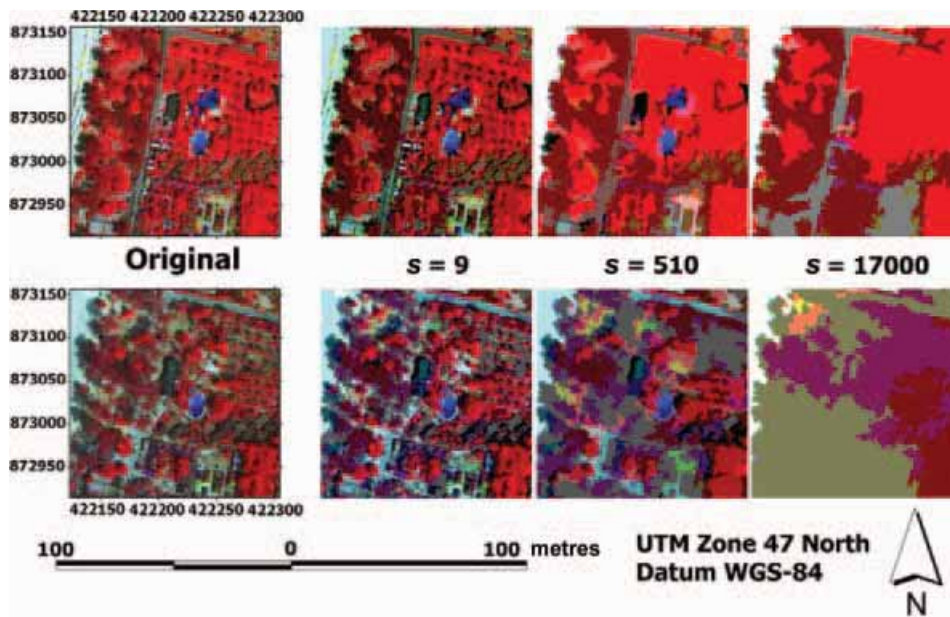


Figure 8. Area morphology scale-space assists visual interpretation. *a)* original false colour composite image, *b)* false colour composite image on scale  $s=9$ , *c)*  $s=510$ , and *d)*  $s=17000$ . Upper plots are from the pre-event image and the lower plots from the post-event image.

scene is repeated. However, the goal here is to map the changes due to the tsunami attack.

For change detection between two scenes, the pre-event appearance of an object was compared to the classified results of the post-event scene on the same scale. All the properties like shape, size and spectral reflectance that might be changed are shown through this comparison. The same set of parameters applied to the post-event scene produced a very messy classified result, especially along the coastline. A street object along Patong Beach, which was segmented between scales 510 and 1167, is picked up for illustration in figure 9. It is presented as a vector polygon overlaying on the pre-event image (figure 9(a)). The classified result of the post-event image on the same range scale, i.e. between 510 and 1167, is shown in figure 9(b). This street was covered by mud or sand and hence disappeared in the post-event scene except for the horizontal branch which was retained, i.e. the long thin green object in the middle of figure 9(b).

Another example is a big vegetation object which is actually an area covered by grass and many trees in a resort (figure 10(a)). Grassland was completely washed away while several trees still stood. As shown in figure 10(b), a big part of this object which is blue and in the middle of the figure shows the same spectral class of mud or sand. Farther inland, the segmented objects showed almost no change such as a vegetation object segmented both from the pre-event and post-event scene (figure 11). This location was confirmed as the farthest point where the tsunami ran up from interviewing local people. For easy-to-observe illustration, each successfully segmented object, as shown in figures 9(a), 10(a) and 11(a) and 11(b), is presented as a transparent polygon with thick and darker coloured boundaries overlaid on a false colour composite image.

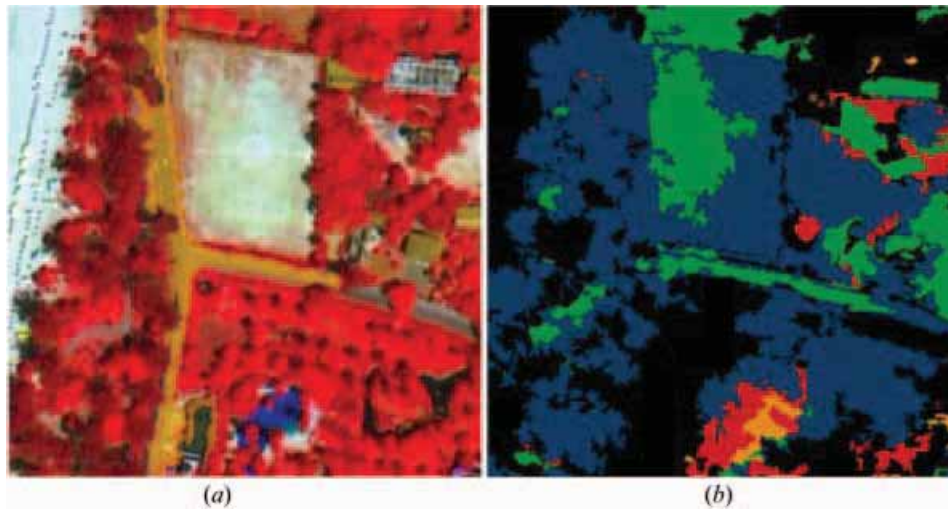


Figure 9. A street object was changed due to the tsunami: (a) extracted objects from the pre-event scene (yellow object overlaid on false colour composite pre-event image) and (b) extracted results from the post-scene on the same scale (between  $s=510$  and  $s=1167$ ) (black for background and colour codes for different spectral classes).

## 6. Conclusion

The dual-scale mapping idea is introduced and applied in order to map 2004 Indian Ocean tsunami-affected areas. Dual-scale mapping targets the reduction of cost and processing time for a quick response after a catastrophe or to offer a cost-effective solution. While macro-scale mapping can provide an affected extent in a large rural area or in a totally devastated area, micro-scale mapping can provide a detailed change of each object because the method possesses higher spatial resolutions.

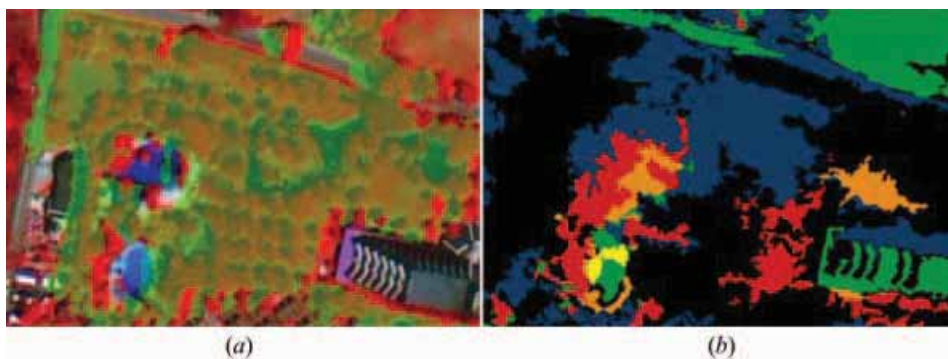


Figure 10. A vegetation object that was changed due to the tsunami: (a) extracted objects from the pre-event scene (green object overlaid on false colour composite pre-event image) and (b) extracted results from the post-event scene on the same scale (between  $s=510$  and  $s=1167$ ) (black for background and colour codes for different spectral classes).

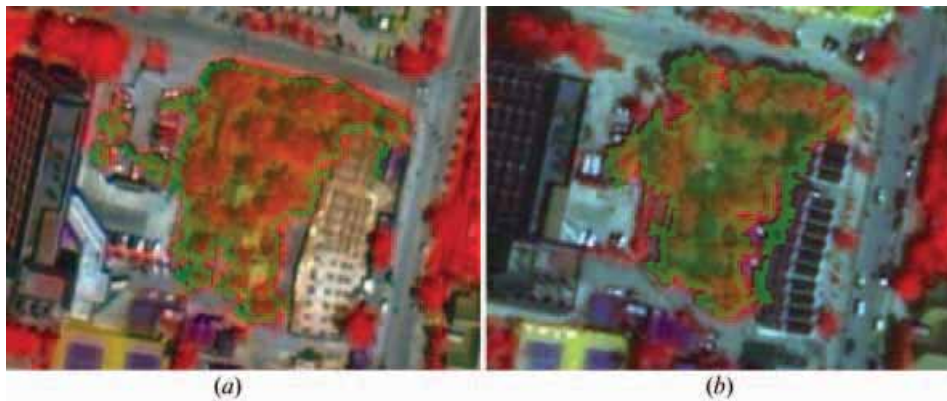


Figure 11. A vegetation object that was retained after the tsunami: (a) extracted from the pre-event scene (green object overlaid on false colour composite pre-event image) and (b) extracted from the post-event scene (green object overlaid on false colour composite post-event image) on the same scale (between  $s=510$  and  $s=1167$ ).

Several new image-processing approaches were also developed and applied in proposed dual-scale processing. These are area morphological filtering, area morphological classification/segmentation, and pan-sharpening *PCPANfit*. Each of them plays a vital role in the proposed processing flow and is applicable to image processing in general. For a further development of the dual-scale mapping system, a GIS-based environment would be essential allowing users to connect to web-based data catalogues in order to search for satellite images prior to processing. Users could search local user databases or other agencies' databases. The idea would also be applicable to mapping or monitoring other natural hazards like floods and earthquakes, etc.

#### Acknowledgement

The QuickBird scenes used in this study are owned by DigitalGlobe Co., Ltd and the SRTM DEM was provided by the US Geological Survey (USGS).

#### References

- AGOURIS, P., CARSWELL, J. and STEFANIDIS, A., 1999, An environment for content-based image retrieval from large spatial database. *ISPRS Journal of Photogrammetry and Remote Sensing*, **54**, pp. 263–272.
- ANDRES, R.J. and ROSE, W.I., 1995, Detection of thermal anomalies at Guatemalan volcanoes using Landsat TM images. *Photogrammetric Engineering and Remote Sensing*, **61**, pp. 775–782.
- BARBER, D.G., HOCHHEIM, K.P., DIXON, R., MOSSCROP, D.R. and McMULLAN, M.J., 1996, The Role of Earth Observation Technologies in Flood Mapping: A Manitoba Case Study. *Canadian Journal of Remote Sensing*, **22**, pp. 137–143.
- CASTELLI, V., BERGMAN, L., KONTOYIANNIS, I., LI, C.-S., ROBINSON, J. and TUREK, J., 1998, Progressive search and retrieval in large image archives. *IBM Journal of Research and Development*, **42**, pp. 253–268.
- EGUCHI, R.T., HUYCK, C.K., HOUSHMAND, B., MANSOURI, B., SHINOZUKA, M., YAMAZAKI, F. and MATSUOKA, M., 2000, The Marmara earthquake: a view from space: the Marmara, Turkey earthquake of August 17, 1999: Reconnaissance Report. Technical Report MCEER-00-0001 (Buffalo, NY: MCEER), pp. 151–169.

- ESTRADA, M., YAMAZAKI, F. and MATSUOKA, M., 2000, Use of Landsat images for the identification of damage due to the 1999 Kocaeli, Turkey earthquake. In *Proceeding of the 21st Asian Conference on Remote Sensing*, 4–8 December 2000, Singapore, pp. 1185–1190.
- LANTUEJOL, C. and MAISONNEUVE, F., 1984, Geodesic methods in image analysis. *Pattern Recognition*, **17**, pp. 117–187.
- LINDBERG, T., 1993, Discrete derivative approximations with scale-space properties: a basis for low-level feature extraction. *Journal of Mathematical Imaging and Vision*, **3**, pp. 349–376.
- MASSONNET, D., ROSSI, M., CARMONA, C., ADRAGNA, F., PELTZER, G., FEIGL, K. and RABAUTE, T., 1993, The displacement field of the Landers earthquake mapped by radar interferometry. *Nature*, **364**, pp. 138–142.
- MATSUOKA, M. and YAMAZAKI, F., 1999, Characteristics of satellite images of damaged areas due to the 1995 Kobe earthquake. In *Proceedings of the 2nd Conference on the Applications of Remote Sensing and GIS for Disaster Management*, 19–21 January 1999, The George Washington University, CD-ROM (Washington DC: George Bernard Shaw University).
- MITOMI, H., SAITA, J., MATSUOKA, M. and YAMAZAKI, F., 2001, Automated damage detection of buildings from aerial television images of the 2001 Gujarat, India earthquake. In *Proceedings of the IEEE 2001 International Geoscience and Remote Sensing Symposium*, 9–13 July, IEEE, CD-ROM, 3p (Piscataway, NJ: IEEE).
- MOUGINIS-MARK, P., ROWLAND, S., FRANCIS, P., FRIEDMAN, T., GRADIE, J., SELF, S., WILSON, L., CRISP, J., GLAZE, L., JONES, K., KAHLE, A., PIERI, D., ZEBKER, H.A., KREUGER, A., WALTER, L., WOOD, C., ROSE, W., ADAMS, J. and WOLFF, R., 1991, Analysis of active volcanoes from the Earth Observing System. *Remote Sensing of Environment*, **36**, pp. 1–12.
- SAITO, K., SPENCE, R.J.S., GOING, C. and MARKUS, M., 2004, Using high-resolution satellite images for post-earthquake building damage assessment: a study following the 26 January 2001 Gujarat earthquake. *Earthquake Spectra*, **20**, pp. 145–169.
- SERRA, J., 1982, *Image Analysis and Mathematical Morphology* (London: Academic Press).
- SINGHROY, V. and MATTAR, K.E., 2000, SAR image techniques for mapping areas of landslides. In *Proceedings of ISPRS Congress*, Amsterdam, 16–22 July 2000, (Enschede: ISPRS), pp. 1395–1402.
- SOILLE, P. and PESARESI, M., 2002, Advances in mathematical morphology applied to geoscience and remote sensing. *IEEE Transactions on Geoscience and Remote Sensing*, **40**, pp. 2042–2055.
- TOU, J.T. and GONZALEZ, R.C., 1974, *Pattern Recognition Principles* (Reading, MA: Addison Wesley).
- VINCENT, L., 1992, Morphological area opening and closings for greyscale images. In *Proceedings NATO Shape in Picture workshop*, 7–11 September 1992, Driebergen, The Netherlands (Berlin, Heidelberg: Springer-Verlag), pp. 197–208.
- VINCENT, L., 1994, Fast grayscale granulometry algorithms. In *Proceeding EURASIP Workshop ISMM'94, Mathematical Morphology and its Applications to Image Processing*, 5–9 September 1994, Fontainebleau, France (Dordrecht: Kluwer Academic), pp. 265–272.
- VOHORA, V.K. and DONOGHUE, S.L., 2004, Application of remote sensing data to landslide mapping in Hong Kong. In *Proceeding of ISPRS Congress*, 12–23 July 2004, Istanbul, Turkey, DVD-ROM (Ottawa: ISPRS).
- VU, T.T., MATSUOKA, M. and YAMAZAKI, F., 2005, Detection and animation of damage using very high-resolution satellite data following the 2003 Bam, Iran, earthquake. *Earthquake Spectra*, **21** (S1), pp. S319–S327.
- YAMAZAKI, F., YANO, Y. and MATSUOKA, M., 2005, Visual damage interpretation of buildings using QuickBird images following the 2003 Bam, Iran, earthquake. *Earthquake Spectra*, **21** (S1), pp. S329–S336.

- ZHANG, Y., 2002, Problems in the fusion of commercial high-resolution satellite images as well as Landsat 7 images and initial solutions. In *Proceeding of Joint International Symposium on GeoSpatial Theory, Processing and Applications*, 8–12 July, 2002, Ottawa, Canada.